Separation and Purification Technology 283 (2022) 120220

Contents lists available at ScienceDirect

Separation and Purification Technology

journal homepage: www.elsevier.com/locate/seppur

Highly selective gas separation by two isostructural boron cluster pillared MOFs

Wanqi Sun [a], Jianbo Hu [b], Simon Duttwyler [c], Lingyao Wang [a,c,*], Rajamani Krishna [d,*], Yuanbin Zhang [a,b,*]

[a] Key Laboratory of the Ministry of Education for Advanced Catalysis Materials, College of Chemistry and Life Sciences, Zhejiang Normal University, Jinhua 321004, PR China
[b] College of Chemical and Biological Engineering, Zhejiang University, Hangzhou 310027, PR China
[c] Department of Chemistry, Zhejiang University, Hangzhou 310027, PR China
[d] Van't Hoff Institute for Molecular Sciences, University of Amsterdam, Science Park 904, 1098 XH Amsterdam, Netherlands

ARTICLE INFO

Keywords:
Gas separation
Metal–organic frameworks
Dodecaborate
Acetylene capture
Carbon dioxide

ABSTRACT

Two isostructural *closo*-dodecaborate $[B_{12}H_{12}]^{2-}$ pillared metal organic frameworks (MOFs), BSF-4 and BSF-9, were synthesized and compared in the performance of selective gas adsorption and separation. BSF-9 with symmetrical interpenetration and two contracted 1D channel exhibited efficient uptake of C_2H_2 (85.1/76.3 mLg^{-1}, 278/298 K) with high separation selectivity over C_2H_4 (41.4, 298 K), outperforming BSF-4 (7.3, 298 K) and many benchmark MOFs. The selectivity of C_2H_6/CH_4, CO_2/CH_4, CO_2/N_2 on BSF-9 (25.2, 9.9, 56.6) and BSF-4 (19.0, 8.9, 41.7) was all relatively high and comparable. The practical gas separation ability for C_2H_2/C_2H_4 mixtures on BSF-9 was confirmed by mixed gas breakthrough experiments with negligible capacity loss after 4 cycles, indicating its potential for purification of ethylene from acetylene-containing industrial gas mixtures. The C_2H_2 and C_2H_4 bonding sites and bonding energies within the framework of BSF-9 were further compared by density functional theory (DFT) study, indicating that C_2H_2 can be trapped tightly between two anionic $[B_{12}H_{12}]^{2-}$ by four synergistic dihydrogen bonds while C_2H_4 only interacts with single $[B_{12}H_{12}]^{2-}$ with weaker bonding energy. BSF-4 with asymmetrical interpenetration and single extended 1D channel showed higher selectivity of C_3H_8/CH_4 (138.5, 298 K) than that of BSF-9 (64.0, 298 K). Inverse ambient adsorption capacity of $C_3H_8 < C_2H_6$ was observed in BSF-9 due to the small pore window and 1D channel.

1. Introduction

The separation of light hydrocarbon mixtures into each pure component is an important but energy-consuming process in the petrochemical industry [1]. Ethylene (C_2H_4) is the foremost olefin in the world with an annual production capacity over 170 million metric tons in 2018 [2]. It is mainly produced by steam cracking, during which a small amount of acetylene (C_2H_2) is produced and needs to be removed to $<$ 40 ppm for avoiding catalyst poisoning during polymerization owning to the formation of metal acetylide [3]. However, the separation of C_2H_2 from C_2H_4 represents one of the most challenging tasks due to the similarity of their physical and chemical properties [4]. Conventional approaches for C_2H_2/C_2H_4 separation relying on cryogenic distillation, partial hydrogenation or solvent extraction are either highly energy-intensive or associated with pollution. Therefore, it is necessary to develop effective, sustainable, and energy-efficient alternative technologies for the removal of trace C_2H_2. On the other hand, natural gas (NG) has become a promising clean energy source to replace the conventional fossil fuels due to its natural abundance and environmental friendliness, which consists mainly of methane (75–90%) [5]. Besides methane, a small amount of C_2H_6, C_3H_8, and CO_2 (totally 0–20%) exist in the NG as well. To improve the quality of NG and recover C_2H_6 and C_3H_8, efficient separation of C_2H_6 and C_3H_8 from CH_4 is a prerequisite [6] (see Table 1).

Adsorption-based separation using porous solid materials is a promising alternative method for efficient separation and purification of hydrocarbon mixtures [7]. Porous metal–organic frameworks (MOFs) constructed by metal-ions/clusters and organic linkers are potential

* Corresponding authors at: Key Laboratory of the Ministry of Education for Advanced Catalysis Materials, College of Chemistry and Life Sciences, Zhejiang Normal University, Jinhua 321004, PR China (Y. Zhang).
E-mail addresses: lywang@zjnu.edu.cn (L. Wang), r.krishna@contact.uva.nl (R. Krishna), ybzhang@zju.edu.cn (Y. Zhang).

https://doi.org/10.1016/j.seppur.2021.120220
Received 19 October 2021; Received in revised form 21 November 2021; Accepted 25 November 2021
Available online 30 November 2021
1383-5866/© 2021 Elsevier B.V. All rights reserved.

Table 1
Dual-site or single-site Langmuir parameter fits.

MOFs	Gases	$q_{A,sat}$	b_{A0}	E_A	$q_{B,sat}$	b_{B0}	E_B
BSF-9	C_3H_8	15.98	9.94E-13	58.43	18.34	2.30E-06	31.34
	C_2H_6	34.49	1.03E-09	34.10	–	–	–
	CH_4	42.15	3.20E-07	22.58	–	–	–
	C_2H_2	56.56	1.08E-9	50.5	31.36	1.57E-9	40.46
	C_2H_4	18.82	1.203E-14	65.5	33.6	1.26E-7	34.4
	N_2	37.81	4.63E-7	17.69	–	–	–
BSF-4	C_3H_8	27.79	1.83E-08	43.7	13.49	3.49E-09	36.73
	C_2H_6	36.53	5.28E-08	34.77	–	–	–
	CH_4	41.17	4.14E-07	21.97	–	–	–

adsorbents for this application due to their modular nature with controllable pore aperture and surface environment [8]. In the context of light hydrocarbon separation, a plenty of MOFs with specific H-bonding acceptors (-F, -Cl –OH, $–NH_2$) [9] or coordinatively unsaturated open metal sites (OMSs) [10] have been developed, such as SIFSIX-2-Cu-i [9a], NKMOF-1-Ni [10a], and MOF-74 [10b]. Compared to the well developed highly electronegative -F, –OH, $–NH_2$ groups, the modestly electronegative B-$H^{\delta-}$ group has less been used for the selective recognition of polar hydrocarbon molecules from less polar hydrocarbon molecules mainly due to the lack of MOFs featuring B-$H^{\delta-}$ functionality [11].

In 2019, we reported the first example (BSF-1) of anionic boron cluster pillared supramolecular metal–organic frameworks (BSFs) by self-assembly of Cu^{2+}, $B_{12}H_{12}^{2-}$ anion and 1,2-bis(4-pyridyl)acetylene linkers [12]. Since then, our interests continually focus on the design and preparation of new BSFs [13]. Through extending the organic ligand length, a isoreticular MOF named as BSF-3 with the composition of $CuB_{12}H_{12}(dpb)_2$ (dpb = 1,4-di(pyridin-4-yl)benzene) could be generated [13b]. Compared to BSF-1, BSF-3 exhibited much increased C_2H_2 capacity and selectivity over C_2H_4 and CO_2, which was one of the best materials for separation of C_2H_2/C_2H_4 and C_2H_2/CO_2 at that time. Very recently, we designed the first example (BSF-9, also termed also ZNU-1) of symmetrically interpenetrated BSFs, which exhibited the record C_2H_2/CO_2 selectivity among all the robust materials without open metal sites [13f]. At 298 K and 0.01 bar, the C_2H_2 uptake on BSF-9 was 1.22 mmol/g, much higher than those from BSF-3 (0.77 mmol/g) and many other benchmark materials. Herein, we would like to detailed investigate the separation performance of other gas mixtures in BSF-9 and compare it with its isostructural analogue BSF-4 (Fig. 1). BSF-9 and BSF-4 feature similar single network due to the close length and shape of organic linkers (9.3 Å for BSF-9 and 9.0 Å for BSF-4). However, BSF-9 is symmetrically interpenetrated while BSF-4 features asymmetric interpenetration as other BSFs. Therefore, two pores are accessible in BSF-9 while only the largest pore is useful in BSF-4. The results showed that BSF-9 exhibited remarkable C_2H_2/C_2H_4 separation performance. The calculated ideal adsorbed solution theory (IAST) selectivity for 1/99 C_2H_2/C_2H_4 and 50/50 C_2H_2/C_2H_4 was 10.2–19.7 and 11.3–41.4, superior to those of many popular MOFs. The binding configurations and bonding energies (ΔE) of C_2H_2 and C_2H_4 calculated by density functional theory (DFT) study indicated that C_2H_2 was tightly trapped by four H-bonding acceptors from two opposite dodecaborates with ΔE of 56.9 kJ/mol while C_2H_4 only interacted with single dodecoborate with decreased ΔE of 44.1 kJ/mol. The practical separation of C_2H_2/C_2H_4 was demonstrated by breakthrough experiments with good recycability. Moreover, BSF-9 showed slightly improved IAST selectivity of C_2H_6/CH_4, CO_2/CH_4, and CO_2/N_2 compared to BSF-4. However, the capacity of C_3H_8 as well as the selectivity of C_3H_8/CH_4 (144.6–114.1) are much higher in BSF-4, which is probably due to the contract pore window of BSF-9 (Fig. 1b). Notably, the capacity of C_2H_6 is higher than that of C_3H_8 in BSF-9, which has rarely been reported. Such abnormal phenomenon is also resulted from the small pore windows that hinder large molecules to pass through.

2. Experimental

2.1. Preparation of BSF-4 and BSF-9

The detailed procedure for the synthesis of BSF-4 and BSF-9 could be found in our recently reported work [13c, f]. The detailed basic characterization of those two MOFs has also been reported there.

2.2. Adsorption measurements

The gas adsorption measurements were performed on a Builder SSA 7000 (Beijing) instrument with two separated stations. Before gas adsorption measurements, the sample was evacuated at 70 °C for 24 h until the pressure dropped below 0.1 Pa.

2.3. Fitting of pure component isotherms

The adsorption isotherms in BSF-9 and BSF-4 were fitted using a dual-site Langmuir model (or single-site Langmuir model):

$$q = \frac{q_{sat,A} b_A p}{1 + b_A p} + \frac{q_{sat,B} b_B p}{1 + b_B p} \quad (1)$$

P is the pressure of the bulk gas at equilibrium with the adsorbed phase (kPa), q is the adsorbed amount per mass of adsorbent (STP mL g^{-1}), $q_{A,sat}$ and $q_{B,sat}$ are the saturation capacities of site A and B (STP mL g^{-1}), b_A and b_B are the affinity coefficients of site A and B (kPa^{-1}). For

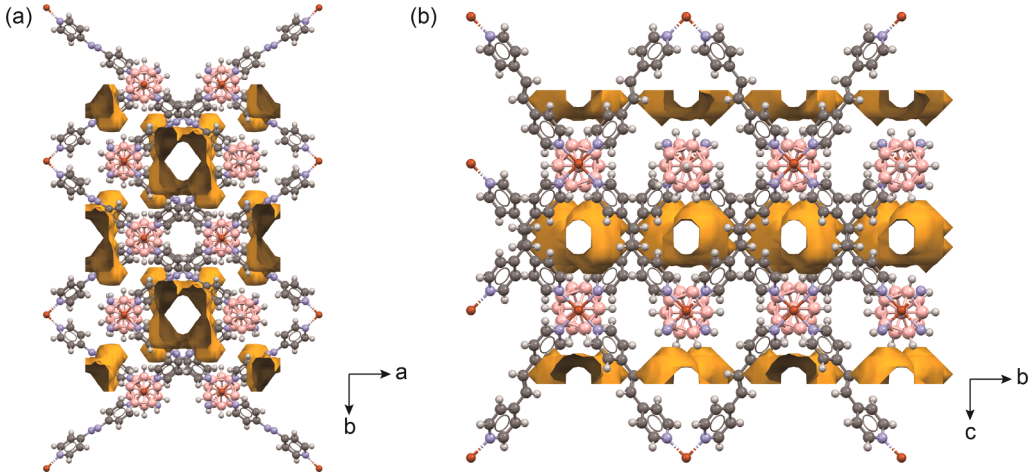

Fig. 1. Crystal structure of BSF-4 and BSF-9 with unit cells of 1 × 2 × 1. Voids are generated with a probe radius of 1.2 Å.

single-site Langmuir model, $q_{B,sat} = 0$.

In eq (1), the Langmuir parameters b_A, b_B are both temperature dependent

$$b_A = b_{A0} exp\left(\frac{E_A}{RT}\right); \quad b_b = b_{B0} exp\left(\frac{E_B}{RT}\right) \tag{2}$$

In eq (2), E_A, E_B are the energy parameters associated with sites A, and B

All the adsorption isotherms are fitted with excellent accuracy ($R^2 > 0.99$). The dual-site or single-site Langmuir parameter fits for gases in BSF-9 and BSF-4 are shown below (Table 1).

The isosteric heat of adsorption, Q_{st}, is defined as

$$Q_{st} = -RT^2\left(\frac{\partial lnp}{\partial T}\right)_q \tag{3}$$

The derivative in the right member of eq (3) is determined at constant adsorbate loading, q (STP mL g^{-1}). The calculations are based on the use of the Clausius-Clapeyron equation.

The IAST adsorption selectivity for two gases is defined as:

$$S_{ads} = \frac{q_1/q_2}{y_{10}/y_{20}} \tag{4}$$

Here, q_1, and q_2 are the loadings in the adsorbed phase in equilibrium. y_{10}, y_{20} are the mole fractions of the bulk gas phase mixture.

2.4. Methods for simulated breakthrough curves

Transient breakthrough simulations of the adsorption were carried out for 1/99 C_2H_2/C_2H_4 mixtures, CO_2/N_2 (15/85) mixtures, $C_3H_8/C_2H_6/CH_4$ (5/10/85) mixtures, operating at a total pressure of 100 kPa and 298 K, using the methodology described in earlier publications [13f]. For comparing the separation performance of MOFs, simulations of transient desorption are carried out under these conditions: cross-sectional area, A = 1 m^2; superficial gas velocity at the entrance to the bed, 0.04 m s^{-1}; voidage of the packed bed = 0.4, the mass of the adsorbent in the bed = 180 kg.

2.5. Dynamic breakthrough experiments

The breakthrough experiments were conducted in a dynamic gas breakthrough equipment using a stainless steel column (Φ 1 cm inner diameter × 20 cm length). The weight of BSF-9 packed in the column was 2.14 g. The column packed with sample was first purged with a Ar flow (5 mL min^{-1}) for 12 h at 75 °C. Then a 1/99 C_2H_2/C_2H_4 gas mixture was introduced. Outlet gas from the column was monitored using gas chromatography (GC-9860-5CNJ, Shanghai) with the thermal conductivity detector TCD. After the breakthrough experiment, the sample was regenerated with Ar purge for second use.

2.6. DFT calculation

The DFT calculation were performed using the Gaussian package. The PBE0 functionals with the Grimme's D3(BJ) dispersion correction were applied to DFT calculations along with the 6–311 + G(d, p) basis set. All structures were optimized without any symmetry constraints and the optimized minimum-energy structures were verified as stationary points on the potential energy surface by performing numerical harmonic vibrational frequency calculations. The equation for the calculation of binding energy (ΔE) is defined as: ΔE = E (BSF + gas) – [E (BSF) + E (gas)].

3. Results and discussion

3.1. C_2H_2/C_2H_4 separation

Single component C_2H_2 adsorption measurements were conducted at 273, 278, 283, 288, 293, 298, 303 and 308 K for BSF-9 after activation, which all showed Type I isotherms with steep slopes under low pressure range (Fig. 2a). The C_2H_2 uptakes at 0.01 bar were relatively high and the values were 48.6, 44.0, 40.3, 36.6, 32.7, 26.2, 22.2, 16.1 mL/g, respectively. At 1.0 bar, the C_2H_2 uptakes were 82.5, 76.3, and 69.1 mL/g at 288, 298, and 308 K respectively. When compared, C_2H_4 adsorption isotherms was less steep and the C_2H_4 capacities were 41.2, 37.1, and 32.2 mL/g respectively (Fig. 2b). Notably, the C_2H_2/C_2H_4 uptake ratio in BSF-9 at 0.01 bar were as high as 10, superior to many leading materials such as BSF-3 (5) [13b] and NKMOF-1-Ni (4) [10a]. The isosteric enthalpy of adsorption (Q_{st}) for BSF-9 was then calculated using the Clausius − Clapeyron equation. Q_{st} values at very low loading for C_2H_2 and C_2H_4 were 54 and 35 kJ/mol (Fig. 2c), well consistent with the static isotherms. The Q_{st} values for C_2H_4 were increased rapidly after the gas loading was over 1.0 mmol/g, which is probably due to the close packing of C_2H_4 molecules in the contract pores that leads to the enhanced guest–guest interactions.

The selectivity for C_2H_2/C_2H_4 (50/50 and 1/99) gas mixtures on BSF-9 at 298 K was calculated using ideal adsorbed solution theory (IAST) after fitting isotherms to the dual-site Langmuir equation with excellent accuracy ($R^2 > 0.998$). At 1.0 bar, the IAST selectivity for equimolar C_2H_2/C_2H_4 mixtures is 41.4 (Fig. 2d), superior to BSF-4 (7.5) [13c], BSF-3 (13.0) [13b], BSF-3-Co (10.2) [13b], BSF-2 (2.9) [13a], BSF-1 (2.4) [12] and many other popular MOFs such as TIFSIX-2-Ni-i (16.3) [14], JCM-1 (13.2) [15], M'MOF-3a (34.2) [16], UTSA-100a (19.6) [17], SIFSIX-2-Cu-i (41.0) [9a] and SIFSIX-1-Cu (10.63) [9a] (Table 2). The IAST selectivity for 1/99 C_2H_2/C_2H_4 in BSF-9 at 1.0 bar is decreased to 19.7, but still much higher than those of BSF-3-Co (8.5) and BSF-3 (8.1) (Fig. 2e) as well as many leading materials such as ELM-12 (14.8) [18], UTSA-100a (10.72) [17], SIFSIX-3-Zn (8.82) [9a], SIFSIX-3-Ni (5.03) [9a], SIFSIX-1-Cu (10.63) [9a], SIFSIX-2-Cu (6.0) [9a], NOTT-300 (2.17) [19] and FeMOF-74 (2.08) [20] (Table 2). The higher IAST selectivity for 1/99 mixtures than for 50/50 mixtures is consistent with the high affinity of BSF-9 to C_2H_2 under low pressures but decreased uptake ratios of C_2H_2/C_2H_4 under high pressures. The C_2H_2 and C_2H_4 uptake capacities from C_2H_2/C_2H_4 mixture were calculated based on IAST model, which indicated that the C_2H_2 uptakes from 50:50 and 1:99 mixtures were 3.05 and 0.29 mmol/g (Fig. 2f).

studies using dispersioncorrected density functional theory (DFT-D) calculations were conducted (Fig. 3). C_2H_2 was tightly trapped by four H-bonding acceptors from two opposite dodecaborates. The four B-$H^{\delta-}\cdots H^{\delta+}$-C distances were 2.183, 2.263, 2.285, and 2.397 Å, respectively. The calculated bonding energy (ΔE) was as high as 56.9 kJ/mol. In sharp contrast to C_2H_2 adsorption configuration, C_2H_4 was observed to only interact with the dodecoborate anion from single side with B-$H^{\delta-}\cdots H^{\delta+}$-C distances of 2.311 and 2.399 Å. The B-$H^{\delta-}\cdots H^{\delta+}$-C distances between C_2H_4 and dodecaborate on the other side were 2.439 and 2.804 Å, beyond the definition of dihydrogen bonds (≤2.4 Å). However, a close contact between C_2H_4 and pyridyl groups were observed with B-$H^{\delta-}\cdots\pi$ distance of 2.867 Å. The calculated bonding energy between C_2H_4 and BSF-9 was 44.1 kJ/mol, much lower than that for C_2H_2 adsorption, which is highly consistent with the experimental results.

To evaluate the practical feasibility of BSF-9 for selective C_2H_2 capture from the binary C_2H_2/C_2H_4 mixture, experimental breakthrough studies were conducted. A gas mixture of C_2H_2/C_2H_4 (1/99) was passed over a tubular column packed with activated BSF-9 solid at 298 K with a flow rate of 5 mL/min. The breakthrough curve depicted in Fig. 4a clearly demonstrated that BSF-9 could remove trace C_2H_2 from C_2H_4 under dynamic conditions in an effective manner. C_2H_4 with a lower affinity for BSF-9 appeared at the outlet of column at 10.5 min. The flow of pure C_2H_4 at the outlet continued until the mass-transfer

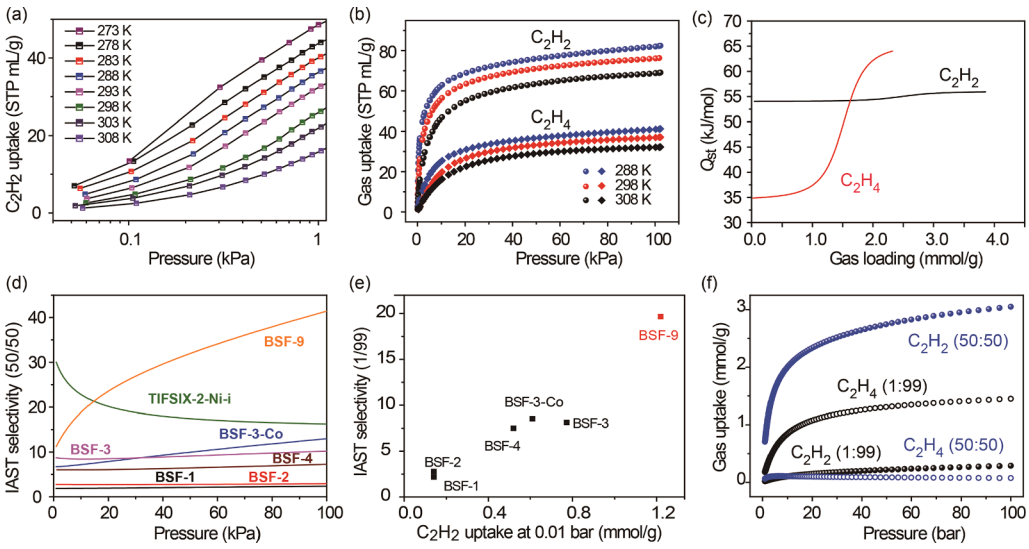

Fig. 2. Static gas adsorption data. (a) C_2H_2 adsorption isotherms in BSF-9 at 273–308 K in the pressure range of 0–1 kPa. (b) C_2H_2 and C_2H_4 adsorption isotherms in BSF-9 at 288–308 K in the pressure range of 0–105 kPa. (c) The isosteric heat of adsorption, Q_{st}, for C_2H_2 and C_2H_4 in BSF-9. (d) C_2H_2/C_2H_4 (50:50) IAST adsorption selectivity comparison. (e) Comparison of the C_2H_2/C_2H_4 (1:99) IAST selectivity and C_2H_2 capacity under low pressure. (f) Calculated gas uptake from C_2H_2/C_2H_4 mixture.

Table 2
Comparison of the C_2H_2 and C_2H_4 uptake capacities and IAST selectivity among popular MOFs To understand the adsorption difference between C_2H_2 and C_2H_4, modeling

Porous Materials	C_2H_2 uptake (cm^3/g)	C_2H_4 uptake (cm^3/g)	C_2H_2/C_2H_4 Selectivity (100 kPa, 298 K)		Ref
			50:50	1:99	
BSF-1	52.6	36.5	2.4	2.2	[12]
BSF-2	41.4	29.6	2.9	2.8	[13a]
BSF-3-Co	86.2	56.2	10.2	8.5	[13b]
BSF-3	81.8	53.1	13.0	8.1	[13b]
BSF-4	53.3	34.9	7.3	–	[13c]
TIFSIX-2-Ni-i	94.3	54.2	16.3	22.7	[14]
JCM-1	76.5	38.1	13.2	8.1	[15]
UTSA-100a	95.65	37.18	19.6	10.72	[17]
SIFSIX-1-Cu	190.4	92.0	4.95	6.0	[9a]
SIFSIX-2-Cu-i	90.0	49.1	41.01	44.54	[9a]
M'MOF-3a	42.5	8.96	34.2	20.03	[18]
ELM-12	57.3	22.5	~28	14.8	[10]
SIFSIX-3-Zn	81.53	50.18	13.72	8.82	[9a]
SIFSIX-3-Ni	73.92	39.2	5.98	5.03	[9a]
NOTT-300	142.01	94.97	2.3	2.17	[19]
FeMOF-74	152.3	136.64	2.1	2.08	[20]
CoMOF-74	183	157	1.62	1.7	[20]
FJU-22a	114.8	85.8	–	25.8	[21]
NKMOF-1-Ni	61	47.3	–	~50	[10a]
PCP-33	121.8	86.8	~3	–	[22]
BSF-9	76.3	37.1	41.4	19.7	This work

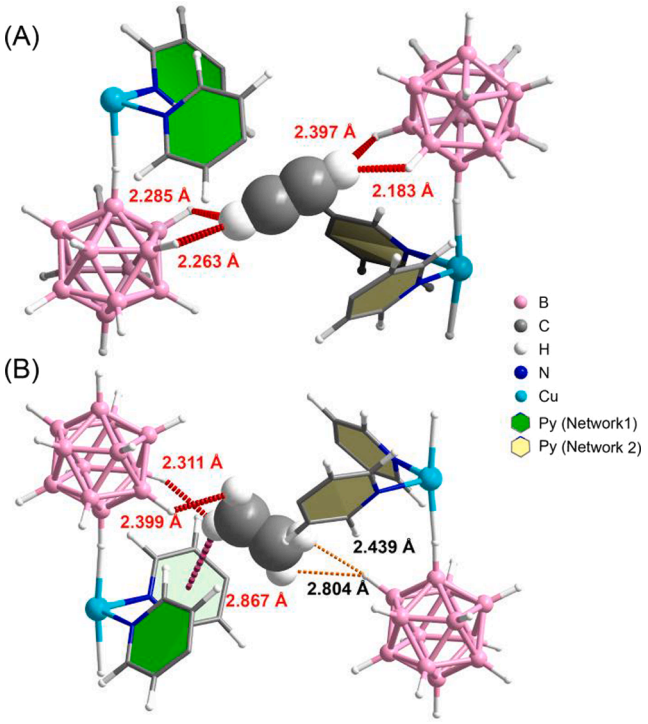

Fig. 3. Comparison of the DFT-D optimized adsorption configurations of C_2H_2 (A) and C_2H_4 (B) in BSF-9.

zone of C_2H_2 that propagated along the column reached the end of the column at 85.5 min. This large breakthrough time difference indicated the excellent separation performance of BSF-9 for C_2H_2/C_2H_4 mixtures. The regeneration conditions for BSF-9 after saturation of the C_2H_2/C_2H_4 gas mixture were tested. After the completion of the breakthrough experiments, the column was purged with a Ar flow (5 mL/min) at 348 K and the outlet gas concentration was monitored. The results showed that the outlet concentration of C_2H_4 and C_2H_2 reduced to a very low concentration (<100 ppm) within 2 h, which indicated the easy regeneration of BSF-9 (Fig. 4b). The breakthrough experiments were repeated for 4 times and the performance of BSF-9 was almost invariable over 4 adsorption–desorption cycles, indicating the good recycability of BSF-9 for C_2H_2 capture. The experimental breakthrough curves were compared with the simulated one under similar conditions (Fig. 4c). The simulated breakthrough curves are slightly sharper due to the neglect of the intra-crystalline diffusion in simulation, indicating that small diffusional influences exist in the real breakthrough experiments. Otherwise, these two curves matched with each other very well.

3.2. CO_2/N_2 separation

The capture of CO_2 from N_2 in flue gas is important to reduce the emission of greenhouse gas into the atmosphere [23]. In this context, a plenty of MOFs have been developed to selective separation of CO_2 (kinetic molecular diameter 3.3 Å) and N_2 (kinetic molecular diameter 3.65 Å) [24]. However, MOFs with suitable pores for molecular sieving of CO_2 from N_2 are rare. Considering the electronagetive boron cluster that can interact with polar molecules by electrostatic interaction as well as the small pore windows in BSF-4 and BSF-9, we would like to

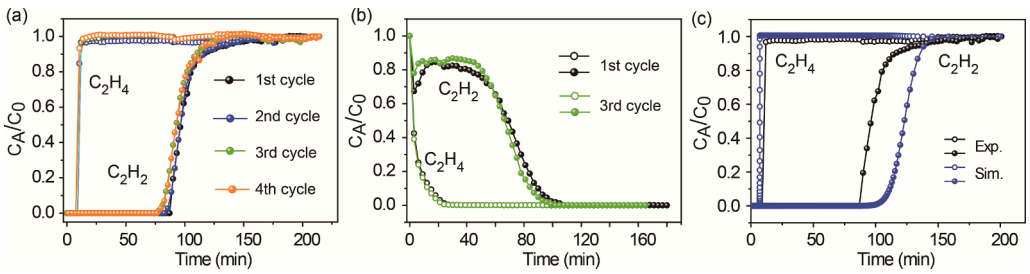

Fig. 4. The breakthrough data. (a) Breakthrough curves of C_2H_2/C_2H_4 (1/99) mixtures at 298 K on BSF-9 for 4 repetitive cycles. (b) Regeneration test of BSF-9 by purging a Ar flow (5 mL/min) at 348 K. (c) Comparison of the simulated and experimental breakthrough curves.

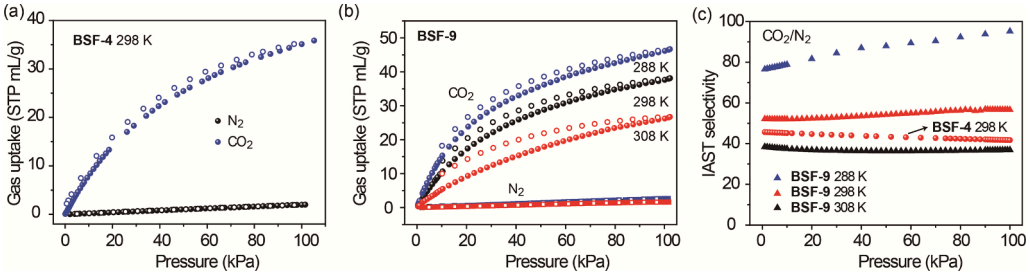

Fig. 5. (a) CO_2 and N_2 adsorption and desorption isotherms at 298 K in BSF-4. (b) CO_2 and N_2 adsorption and desorption isotherms at 288, 298 and 308 K in BSF-9. (c) Calculated IAST selectivity of CO_2/N_2 (50/50) mixture in BSF-4 and BSF-9.

investigate the separation selectivity of CO_2/N_2 in these two BSFs. BSF-4 took up 35.8 mL/g of CO_2 at 298 K and 1 bar but only adsorbed 2.0 mL/g of N_2 (Fig. 5). Similarly, BSF-9 took up 38.1 mL/g of CO_2 and 2.1 mL/g of N_2 under the same conditions. Slight hysteresis was observed for the desorption curves due to the relatively high affinity of the BSFs towards CO_2. The calculated IAST selectivity is 56 in BSF-9 and 42 in BSF-4 for equimolar CO_2/N_2 mixtures. For 15/85 CO_2/N_2 mixtures that are related to the composition of flue gas, the calculated IAST selectivity is 53 in BSF-9 and 44 in BSF-4. Therefore, both materials showed extremely high selectivity to capture CO_2 from N_2. Such selectivity is higher than those of many popular MOFs such as MIL-53(Al) (10.1) [25], UiO-67 (9.4) [26], BUT-11 (31.5) [26] and ZIF-81 (24.0) [27]. We also measured the CO_2 and N_2 adsorption isotherms in BSF-9 at 288 and 308 K. The calculated selectivity is 99 at 288 K and 37 at 308 K. The simulated breakthrough curves for BSF-9 and BSF-4 further confirmed the superior selectivity of BSF-9 compared to BSF-4 (Fig. 6).

3.3. $C_3H_8/C_2H_6/CH_4$ separation

Natural gas (NG) has been considered as a cleaner energy alternative to other automobile fuels such as gasoline and diesel [28]. The consumption is over 3.1 trillion cubic meters per year globally. In general, NG mainly consists of methane (CH_4), ethane (C_2H_6) and propane

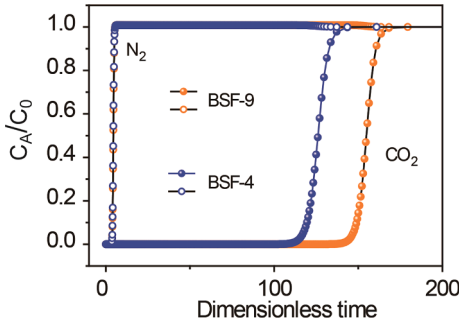

Fig. 6. Comparison of the simulated breakthrough curves of CO_2/N_2 (15/85) for BSF-9 and BSF-4.

(C_3H_8). To fully utilize them, the separation is necessary. In this context, we would like to study the $C_3H_8/C_2H_6/CH_4$ adsorption and separation selectivity in BSF-4 and BSF-9. For all the three gases, the adsorption isotherms are collected at 288, 298, and 308 K (Fig. 7a-f). In BSF-4, the C_3H_8 capacities are 36.2, 34.0, and 32.3 mL/g from 288 to 308 K. The C_2H_6 capacities were slightly lower under each temperatures and the CH_4 uptakes were<1/3 of those for C_3H_8. Such uptake trend (C_3H_8 > C_2H_6 > CH_4) is consistent with those of nearly all the reported materials [29]. In BSF-9, the gas uptake trend is obviously different. While the uptakes of CH_4 is still very low, the uptakes of C_2H_6 are all higher than those of C_3H_8 at 100 kPa from 288 to 308 K although the uptakes of C_3H_8 are higher under very low pressure ranges (<20 kPa). These unusual phenomena can be explained by: 1) C_3H_8 have more hydrogen atoms and larger molecular size and can interact with the framework more strongly initially; 2) the pores of BSF-9 are very small, leading to weakened accommodation space for larger molecules under near-saturation pressure. The isosteric enthalpy of adsorption (Q_{st}) of C_3H_8, C_2H_6 and CH_4 in BSF-4 and BSF-9 are all calculated using the Clausius – Clapeyron equation. The corresponding Q_{st} values at near-zero loading were 43.7, 34.8 and 22.0 kJ/mol in BSF-4 and 32.0, 34.1, 22.6 kJ/mol in BSF-9 (Fig. 7g). For both materials, The Q_{st} trend is the same as the capacity trend at 100 kPa. The IAST selectivity for C_3H_8/CH_4 (5/95) and C_3H_8/CH_4 (10/90) gas mixtures on BSF-4 and BSF-9 at 288–308 K was then calculated and compared. BSF-4 showed very high C_3H_8/CH_4 selectivity (258–167 at 288 K, 192–138 at 298 K, and 145–114 at 308 K), much higher than those of BSF-9 and many other porous MOFs such as UiO-67 (74) [29a], JUC-Liu5 (108) [30], MFM-202a (87) [31] and InOF-1 (90) [32]. However, for C_2H_6/CH_4 separation, BSF-9 exhibited slightly higher selectivity (32–29 at 288 K, 27–25 at 298 K, 24–22 at 308), which is also higher than many well-known materials such as BSF-1(23) [12], UiO-67 (8) [27a] and InOF-1 (17) [32]. Additionally, a large kinetic difference between BSF-9 and BSF-4 were observed for C_3H_8 adsorption when we measured their adsorption isotherms at the same time. It takes about 2–3 folds of time to finish the data collection for BSF-9 compared to for BSF-4 (Fig. S1-6). This can also be explained by the smaller pore windows and channels in BSF-9 that hinder the mass transfer. The simulated breakthrough curves for BSF-9 and BSF-4 for $C_3H_8/C_2H_6/CH_4$ (5/10/85) mixtures indicated the better C_3H_8 capture

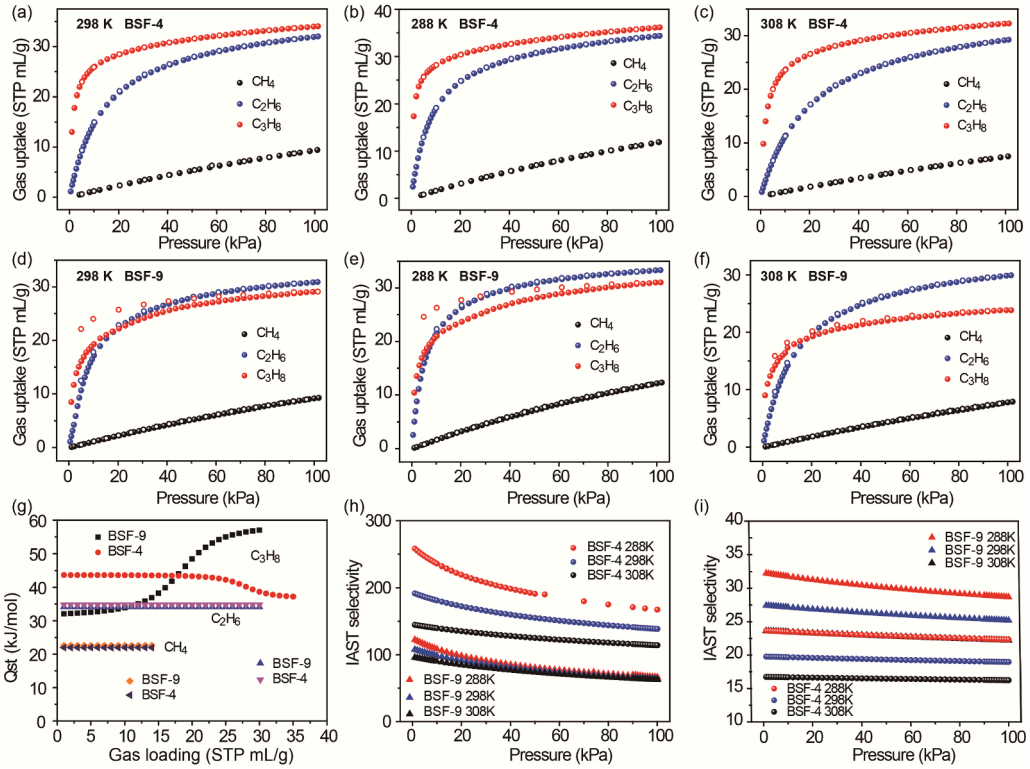

Fig. 7. (a-c) C_3H_8, C_2H_6 and CH_4 adsorption and desorption isotherms at 298, 288 and 308 K in BSF-4. (d-f) C_3H_8, C_2H_6 and CH_4 adsorption and desorption isotherms at 298, 288 and 308 K in BSF-9. (g) The isosteric heat of adsorption, Q_{st}, for C_3H_8, C_2H_6 and CH_4 in BSF-9 and BSF-4. (h) Calculated IAST selectivity of C_3H_8/CH_4 (5/95) mixture in BSF-4 and BSF-9. (i) Calculated IAST selectivity of C_2H_6/CH_4 (10/90) in BSF-4 and BSF-9.

performance in BSF-4, consistent with the static gas adsorption data (Fig. 8). Dynamic breakthrough experiments were also conducted for BSF-9 and BSF-4, which showed that BSF-4 owned the better C_3H_8 capture performance (Fig. S2).

4. Conclusions

In summary, two isostructural ultra-microporous boron cluster pillared metal organic supramolecular frameworks, BSF-4 and BSF-9, constructed by the self-assembly of Cu^{2+}, *closo*-dodecaborate and dipyridyl linkers were synthesized for highly selective separation of C_2H_2/C_2H_4, CO_2/N_2, and $C_3H_8/C_2H_6/CH_4$. Notable features of this work include: 1) remarkable C_2H_2/C_2H_4 selectivity and high C_2H_2 capacity in BSF-9; 2) good dynamic separation performance of C_2H_2/C_2H_4 in BSF-9 with excellent recyclability; 3) reasonable illustration of the C_2H_2 and C_2H_4 adsorption difference by modeling study; 4) high CO_2/N_2 selectivity achieved both by BSF-4 and BSF-9 through near-sieving effect; 5) inverse ambient adsorption capacity of C_3H_8 and C_2H_6 observed in BSF-9; 6) distinct C_3H_8 adsorption kinetics observed for BSF-4 and BSF-9. In general, our work demonstrates the importance of pore size control and boron cluster functionality for efficient gas separation. Other isostructural boron cage hybrid MOFs can be synthesized based on the reticular chemistry [33] or crystal engineering [34] and applied potentially for separation of other fundamental industrial gas/vapor mixtures.

CRediT authorship contribution statement

Wanqi Sun: Methodology, Validation, Investigation. **Jianbo Hu:** Methodology, Investigation. **Simon Duttwyler:** Writing – review & editing, Funding acquisition, Supervision. **Lingyao Wang:** Resources, Supervision, Funding acquisition, Writing – review & editing. **Rajamani Krishna:** breakthrough simulation, Writing – review & editing. **Yuanbin Zhang:** Conceptualization, Methodology, Funding acquisition, Supervision, Writing – original draft.

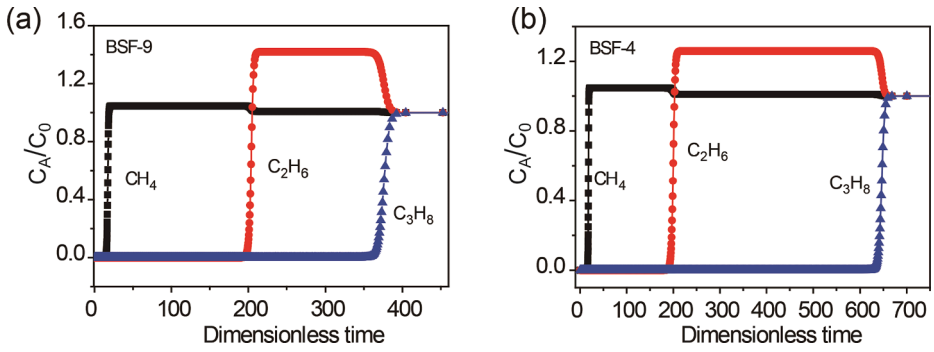

Fig. 8. Comparison of the simulated breakthrough curves of $C_3H_8/C_2H_6/CH_4$ (5/10/85) for BSF-9 (a) and BSF-4 (b).

Declaration of Competing Interest

The authors declare that they have no known competing financial interests or personal relationships that could have appeared to influence the work reported in this paper.

Acknowledgement

This work was supported by the Natural Science Foundation of China (No. 21908193, 21871231, 21850410451).

Appendix A. Supplementary material

Supplementary data to this article can be found online at https://doi.org/10.1016/j.seppur.2021.120220.

References

[1] D.S. Sholl, R.P. Lively, Seven chemical separations to change the world, Nature 532 (7600) (2016) 435–437.

[2] B. Li, X. Cui, D. O'Nolan, H.-M. Wen, M. Jiang, R. Krishna, H. Wu, R.-B. Lin, Y.-S. Chen, D. Yuan, H. Xing, W. Zhou, Q. Ren, G. Qian, M.J. Zaworotko, B. Chen, An Ideal Molecular Sieve for Acetylene Removal from Ethylene with Record Selectivity and Productivity, Adv. Mater. 29 (2017) 1704210.

[3] Y. Chai, X. Han, W. Li, S. Liu, S. Yao, C. Wang, W. Shi, I. da-Silva, P. Manuel, Y. Cheng, L.D. Daemen, A.J. Ramirez-Cuesta, C.C. Tang, L. Jiang, S. Yang, N. Guan, L. Li, Control of zeolite pore interior for chemoselective alkyne/olefin separations, Science 368 (6494) (2020) 1002–1006.

[4] Y. Wang, C. Hao, W. Fan, M. Fu, X. Wang, Z. Wang, L. Zhu, Y. Li, X. Lu, F. Dai, Z. Kang, R. Wang, W. Guo, S. Hu, D. Sun, One-step Ethylene Purification from an Acetylene/Ethylene/Ethane Ternary Mixture by Cyclopentadiene Cobalt-Functionalized Metal-Organic Frameworks, Angew. Chem. Int. Ed. 60 (20) (2021) 11350–11358.

[5] K. Liu, D. Ma, B. Li, Y.i. Li, K. Yao, Z. Zhang, Y.u. Han, Z. Shi, High storage capacity and separation selectivity for C_2 hydrocarbons over methane in the metal-organic framework Cu-TDPAT, J. Mater. Chem. A 2 (38) (2014) 15823–15828.

[6] G. Li, C. Wang, Z. Wang, Structural effects of microporous polymers on adsorption/separation of C_1–C_3 light hydrocarbons and CO_2 in natural gas, Chem. Eng. J. 427 (2022), 131985.

[7] (a) B.R. Barnett, M.I. Gonzalez, J.R. Long, Recent Progress Towards Light Hydrocarbon Separations Using Metal-Organic Frameworks, Trends Chem. 1 (2019) 159–171;
(b) K. Adil, Y. Belmabkhout, R.S. Pillai, A. Cadiau, P.M. Bhatt, A.H. Assen, G. Maurin, M. Eddaoudi, Gas/vapour separation using ultra-microporous metal-organic frameworks: insights into the structure/separation relationship, Chem. Soc. Rev. 46 (2017) 3402–3430;
(c) X. Zhao, Y. Wang, D.-S. Li, X. Bu, P. Feng, Metal-Organic Frameworks for Separation, Adv. Mater. 30 (2018) 1705189;
(d) Y. Wu, B.M. Weckhuysen, Separation and Purification of Hydrocarbons with Porous Materials, Angew. Chem. Int. Ed. 60 (2021) 18930–18949;
(e) J. Gao, X. Qian, R. Lin, R. Krishna, H. Wu, W. Zhou, B. Chen, Mixed Metal-Organic Framework with Multiple Binding Sites for Efficient C2H2/CO2 Separation, Angew. Chem. Int. Ed. 59 (2020) 4396–4400;
(f) J. Gao, Y. Cai, X. Qian, P. Liu, H. Wu, W. Zhou, D. Liu, L. Li, R. Lin, B. Chen, A Microporous Hydrogen-Bonded Organic Framework for the Efficient Capture and Purification of Propylene, Angew. Chem. Int. Ed. 60 (2021) 20400–20406.

[8] (a) P. Liao, N. Huang, W. Zhang, J. Zhang, X. Chen, Controlling guest conformation for efficient purification of butadiene, Science 356 (2017) 1193–1196;
(b) O.T. Qazvini, R. Babarao, S.G. Telfer, Multipurpose Metal-Organic Framework for the Adsorption of Acetylene: Ethylene Purification and Carbon Dioxide Removal, Chem. Mater. 31 (2019) 4919–4926;
(c) F. Luo, C. Yan, L. Dang, R. Krishna, W. Zhou, H. Wu, X. Dong, Y. Han, T.-L. Hu, M. O'Keeffe, L. Wang, M. Luo, R.-B. Lin, B. Chen, UTSA-74: A MOF-74 Isomer with Two Accessible Binding Sites per Metal Center for Highly Selective Gas Separation, J. Am. Chem. Soc. 138 (2016) 5678–5684;
(d) L. Li, R.-B. Lin, R. Krishna, H. Li, S. Xiang, H. Wu, J. Li, W. Zhou, B. Chen, Ethane/ethylene separation in a metal-organic framework with iron-peroxo sites, Science 362 (2018) 443–446;
(e) Y. Zhang, X. Cui, H. Xing, Recent advances in the capture and abatement of toxic gases and vapors by metal-organic frameworks, Mater. Chem. Front. 5 (2021) 5970–6013.

[9] (a) X. Cui, K. Chen, H. Xing, Q. Yang, R. Krishna, Z. Bao, H. Wu, W. Zhou, X. Dong, Y. Han, B. Li, Q. Ren, M.J. Zaworotko, B. Chen, Pore chemistry and size control in hybrid porous materials for acetylene capture from ethylene, Science 353 (2016) 141–144;
(b) X. Liu, Y. Song, C.-X. Zhang, C.-X. Zhao, C. He, Inverse CO2/C2H2 separation in a pillared-layer framework featuring a chlorine-modified channel by quadrupole-moment sieving, Sep. Puri. Technol. 279 (2021), 119608;
(c) W. Yang, A.J. Davies, X. Lin, M. Suyetin, R. Matsuda, A.J. Blake, C. Wilson, W. Lewis, J.E. Parker, C.C. Tang, M.W. George, P. Hubberstey, S. Kitagawa, H. Sakamoto, E. Bichoutskaia, N.R. Champness, S. Yang, M. Schroder, Selective CO2 uptake and inverse CO2/C2H2 selectivity in a dynamic bifunctional metal-organic framework, Chem. Sci. 3 (10) (2012) 2993–2999;
(d) S. Mukherjee, N. Kumar, A.A. Bezrukov, K. Tan, T. Pham, K.A. Forrest, K. A. Oyekan, O.T. Qazvini, D.G. Madden, B. Space, M.J. Zaworotko, Amino-Functionalised Hybrid Ultramicroporous Materials that Enable Single-Step Ethylene Purification from a Ternary Mixture, Angew. Chem. Int. Ed. 60 (2021) 10902–10909.

[10] (a) Y.-L. Peng, T. Pham, P. Li, T. Wang, Y. Chen, K.-J. Chen, K. A. Forrest, B. Space, P. Cheng, M. J. Zaworotko, Z. Zhang, Robust Ultramicroporous Metal-Organic Frameworks with Benchmark Affinity for Acetylene, Angew. Chem. Int. Ed. (57) 2018 10971–10975; (b) J. H. Choe, H. Kim, C.S. Hong, MOF-74 type variants for CO_2 capture, Mater. Chem. Front. 5 (2021) 5172–5185; (c) H. Zeng, M. Xie, Y.-L. Huang, Y. Zhao, X.-J. Xie, J.-P. Bai, M.-Y. Wan, R. Krishna, W. Lu, D. Li, Induced Fit of C_2H_2 in a Flexible MOF Through Cooperative Action of Open Metal Sites, Angew. Chem. Int. Ed. 58 (2019) 8515–8519.

[11] (a) S.-L. Huang, Y.-J. Lin, W.-B. Yu, G.-X. Jin, Porous Frameworks Based on Carborane–Ln2(CO2)6: Architecture Influenced by Lanthanide Contraction and Selective CO2 Capture, ChemPlusChem 77 (2012) 141–147;
(b) O.K. Farha, A.M. Spokoyny, K.L. Mulfort, M.F. Hawthrone, C.A. Mirkin, J. T. Hupp, Synthesis and Hydrogen Sorption Properties of Carborane Based Metal−Organic Framework Materials, J. Am. Chem. Soc. 129 (2007) 12680–12681;
(c) L. Gan, A. Chidambaram, P.G. Fonquernie, M.E. Light, D. Choquesillo-Lazarte, K. Huang, E. Solano, J. Fraile, C. Viñas, F. Teixidor, J.A.R. Naverro, K.C. Stylianou, J.G. Planas, A Highly Water-Stable meta-Carborane-Based Copper Metal-Organic Framework for Efficient High-Temperature Butanol Separation, J. Am. Chem. Soc. 142 (2020) 8299–8311.

[12] Y. Zhang, L. Yang, L. Wang, S. Duttwyler, H. Xing, A Microporous Metal-Organic Framework Supramolecularly Assembled from a Cu^{II} Dodecaborate Cluster Complex for Selective Gas Separation, Angew. Chem. Int. Ed. 58 (2019) 8145–8150.

[13] (a) Y. Zhang, L. Yang, L. Wang, X. Cui, H. Xing, Pillar iodination in functional boron cage hybrid supramolecular frameworks for high performance separation of light hydrocarbons, J. Mater. Chem. A. 7 (2019) 27560–27566;
(b) Y. Zhang, J. Hu, R. Krishna, L. Wang, L. Yang, X. Cui, S. Duttwyler, H. Xing, Rational Design of Microporous MOFs with Anionic Boron Cluster Functionality and Cooperative Dihydrogen Binding Sites for Highly Selective Capture of Acetylene, Angew. Chem. Int. Ed. 59 (2020) 17664–17669;
(c) Y. Zhang, L. Wang, J. Hu, S. Duttwyler, X. Cui, H. Xing, Solvent-dependent supramolecular self-assembly of boron cage pillared metal-organic frameworks for selective gas separation, CrystEngComm 22 (2020) 2649–2655;
(d) L. Wang, T. Jiang, S. Duttwyler, Y. Zhang, Supramolecular Cu(II)-dipyridyl frameworks featuring weakly coordinating dodecaborate dianions for selective gas separation, CrystEngComm 23 (2021) 282–291;
(e) L. Wang, W. Sun, S. Duttwyler, Y. Zhang, Efficient adsorption separation of methane from CO2 and C2–C3 hydrocarbons in a microporous closo-dodecaborate [B12H12]2- pillared metal-organic framework, J. Solid State Chem. 299 (2021), 122167;
(f) L. Wang, W. Sun, Y. Zhang, N. Xu, R. Krishna, J. Hu, Y. Jiang, Y. He, H. Xing, Interpenetration symmetry control within ultramicroporous robust boron cluster hybrid MOFs for benchmark purification of acetylene from carbon dioxide, Angew. Chem. Int. Ed. (2021), https://doi.org/10.1002/anie.202107963.

[14] M. Jiang, X. Cui, L. Yang, Q. Yang, Z. Zhang, Y. Yang, H. Xing, A thermostable anion-pillared metal-organic framework for C_2H_2/C_2H_4 and C_2H_2/CO_2 separations, Chem Eng. J. 352 (2018) 803–810.

[15] J. Lee, C.Y. Chuah, J. Kim, Y. Kim, N. Ko, Y. Seo, K. Kim, T.H. Bae, E. Lee, Separation of Acetylene from Carbon Dioxide and Ethylene by a Water-Stable Microporous Metal-Organic Framework with Aligned Imidazolium Groups inside the Channels, Angew. Chem. Int. Ed. 57 (2018) 7869–7873.

[16] M.C. Das, Q. Guo, Y. He, J. Kim, C.G. Zhao, K. Hong, S. Xiang, Z. Zhang, K. M. Thomas, R. Krishna, B. Chen, Interplay of Metalloligand and Organic Ligand to Tune Micropores within Isostructural Mixed-Metal Organic Frameworks (M′MOFs) for Their Highly Selective Separation of Chiral and Achiral Small Molecules, J. Am. Chem. Soc. 134 (2012) 8703–8710.

[17] T.L. Hu, H. Wang, B. Li, R. Krishna, H. Wu, W. Zhou, Y. Zhao, Y. Han, X. Wang, W. Zhu, Z. Yao, S. Xiang, B. Chen, Microporous metal–organic framework with dual functionalities for highly efficient removal of acetylene from ethylene/acetylene mixtures, Nat. Commun. 6 (2015) 7328–7335.

[18] L. Li, R.-B. Lin, R. Krishna, X. Wang, B. Li, H. Wu, J. Li, W. Zhou, B. Chen, Efficient separation of ethylene from acetylene/ethylene mixtures by a flexible-robust metal–organic framework, J. Mater. Chem. A 5 (2017) 18984–18988.

[19] S. Yang, A.J. Ramirez-Cuesta, R. Newby, V. Garcia-Sakai, P. Manuel, S.K. Callear, S. I. Campbell, C.C. Tang, M. Schröder, Supramolecular binding and separation of hydrocarbons within a functionalized porous metal–organic framework, Nat. Chem. 7 (2014) 121–129.

[20] E.D. Bloch, W.L. Queen, R. Krishna, J.M. Zadrozny, C.M. Brown, J.R. Long, Science, Hydrocarbon Separations in a Metal-Organic Framework with Open Iron(II), Coordination Sites 335 (2012) 1606–1610.

[21] Z. Yao, Z. Zhang, L. Liu, Z. Li, W. Zhou, Y. Zhao, Y. Han, B. Chen, R. Krishna, S. Xiang, Extraordinary Separation of Acetylene-Containing Mixtures with Microporous Metal-Organic Frameworks with Open O Donor Sites and Tunable Robustness through Control of the Helical Chain Secondary Building Units, Chem. - Eur. J. 22 (2016) 5676–5683.

[22] J. Duan, W. Jin, R. Krishna, Natural Gas Purification Using a Porous Coordination Polymer with Water and Chemical Stability, Inorg. Chem. 54 (2015) 4279–4284.

[23] J. Hedlund, G. Garcia, M. Balsamo, M. Zhou, J. Mouzona, Microchannel zeolite 13X adsorbent with high CO_2 separation performance, Sep. Purif. Technol. 277 (2021), 119483.

[24] (a) L. Yang, X. Cui, Y. Zhang, Q. Wang, Z. Zhang, X. Suo, H. Xing, Anion Pillared Meta-Organic Framework Embedded with Molecular Rotors for Size-Selective Capture of CO2 from CH4 and N2, ACS Sustainable. Chem. Eng. 7 (2019) 3138–3144;
(b) L. Yang, X. Cui, Y. Zhang, Q. Wang, Z. Zhang, X. Suo, H. Xing, Anion Pillared Meta-Organic Framework Embedded with Molecular Rotors for Size-Selective Capture of CO2 from CH4 and N2, ACS Sustainable. Chem. Eng. 7 (2019) 3138–3144;
(c) L. Hou, W. Shi, Y. Wang, Y. Guo, C. Jin, Q. Shi, A rod packing microporous metal-organic framework:unprecedented ukv topology, high sorption selectivity and affinity for CO2, Chem. Commun. 47 (2011) 5464–5466;
(d) L. Du, Z. Lu, K. Zheng, J. Wang, X. Zheng, Y. Pan, X. You, J. Bai, Fine-tuning pore size by shifting coordination sites of ligands and surface polarization of metal-organic frameworks to sharply enhance the selectivity for CO2, J. Am. Chem. Soc. 135 (2013) 562–565.

[25] S. Kavak, H.M. Polat, H. Kulak, S. Keskin, A. Uzun, MIL-53(Al) as a Versatile Platform for Ionic-Liquid/MOF Composites to Enhance CO_2 Selectivity over CH_4 and N_2, Chem. Asian J. 14 (2019) 3655–3667.

[26] B. Wang, H. Huang, X.L. Lv, Y. Xie, M. Li, J.R. Li, Tuning CO2 Selective Adsorption over N_2 and CH_4 in UiO-67 Analogues through Ligand Functionalization, Inorg. Chem. 53 (2014) 9254–9259.

[27] R. Banerjee, H. Furukawa, D. Britt, C. Knobler, M. O'Keeffe, O.M. Yaghi, Control of pore size and functionality in isoreticular zeolitic imidazolate frameworks and their carbon dioxide selective capture properties, J. Am. Chem. Soc. 131 (2009) 3875–3877.

[28] K.M.C. Santos, T.R. Menezes, M.R. Oliveira, T.S.L. Silva, K.S. Santos, V.A. Barros, D.C. Melo, A.L. Ramos, C.C. Santana, E. Franceschi, C. Dariva, S.M. Egues, G. R. Borges, J.F. De Conto, Natural gas dehydration by adsorption using MOFs and silicas: A review, Sep. Purif. Technol. 276 (2021), 119409.

[29] (a) Y. Zhang, H. Xiao, X. Zhou, X. Wang, Z. Li, Selective Adsorption Performances of UIO-67 for Separation of Light Hydrocarbons C1/C2/C3, Ind. Eng. Chem. Res. 56 (2017) 8689–8696;
(b) H. Wang, Q. Liu, Y. Wang, S. Yin, A Water-Stable Anionic Metal-Organic Framework Constructed from Columnar Zinc-Adeninate Units for Highly Selective Light Hydrocarbon Separation and Efficient Separation of Organic Dyes, Inorg. Chem. 56 (2017) 2919–2925;
(c) L. Li, X. Wang, J. Liang, Y. Huang, H. Li, Z. Lin, R. Cao, Water-Stable Anionic Metal-Organic Framework for Highly Selective Separation of Methane from Natural Gas and Pyrolysis Gas, ACS Appl. Mater. Interfaces 8 (2016) 9777–9781.

[30] D. Wang, T. Zhao, Y. Cao, S. Yao, G. Li, Q. Huo, Y. Liu, High performance gas adsorption and separation of natural gas in two microporous metal-organic frameworks with ternary building units, Chem. Commun. 50 (2014) 8648–8650.

[31] S. Gao, C.G. Morris, Z. Lu, Y. Yan, H.G.W. Godfrey, C. Murray, C.C. Tang, K. M. Thomas, S. Yang, M. Schröder, Selective Hysteretic Sorption of Light Hydrocarbons in a Flexible Metal-Organic Framework Material, Chem. Mater. 28 (2016) 2331–2340.

[32] Y. Chen, Z. Qiao, D. Lv, H. Wu, R. Shi, Q. Xia, H. Wang, J. Zhou, Z. Li, Selective Adsorption of Light Alkanes on a Highly Robust Indium Based Metal-Organic Framework, Ind. Eng. Chem. Res. 56 (2017) 4488–4495.

[33] (a) H. Lyu, Z. Li, S. Wuttke, O.M. Yaghi, Digital Reticular Chemistry, Chem 6 (2020) 2219–2241;
(b) C. Gropp, S. Canossa, S. Wuttke, F. Gándara, Q. Li, L. Gagliardi, O.M. Yaghi, Standard Practices of Reticular Chemistry, ACS Cent. Sci. 6 (2020) 1255–1273.

[34] (a) A.K. Nangia, G.R. Desiraju, Crystal Engineering: An Outlook for the Future, Angew. Chem. Int. Ed. 22 (2019) 4100–4107;
(b) S. Mukherjee, M.J. Zaworotko, Crystal Engineering of Hybrid Coordination Networks: From Form to Function, Trends Chem. 2 (2020) 506–518.

Supporting Information

Highly selective gas separation by two isostructural boron cluster pillared MOFs

Wanqi Sun,[a] Jianbo Hu,[b] Simon Duttwyler,[c] Lingyao Wang,[ac]* Rajamani Krishna,[d]* Yuanbin Zhang,[ab]*

[a] *Key Laboratory of the Ministry of Education for Advanced Catalysis Materials, College of Chemistry and Life Sciences, Zhejiang Normal University, Jinhua 321004, China.*

[b] *College of Chemical and Biological Engineering, Zhejiang University, Hangzhou 310027, P.R. China.*

[c] *Department of Chemistry, Zhejiang University, Hangzhou 310027, P.R. China*

[d] *Van't Hoff Institute for Molecular Sciences, University of Amsterdam, Science Park 904, 1098 XH Amsterdam, Netherlands.*

*Corresponding authors.

Email address:lywang@zjnu.edu.cn (L. W), r.krishna@contact.uva.nl (R. K.), ybzhang@zju.edu.cn (Y. Z).

Table S1. Raw data for C_3H_8 adsorption isotherms of BSF-9 at 298 K

	Adsorption			
SN	Pressure [KPa]	Relative pressure [P/Po]	Volume [cc/g]	Time [H:M:S]
1	1.031600	1.0114E-02	8.454302	01:38:54
2	2.045882	2.0058E-02	11.656582	02:13:30
3	3.085272	3.0248E-02	13.834328	02:49:27
4	4.100634	4.0202E-02	15.055773	03:08:51
5	5.102458	5.0024E-02	16.090193	03:27:21
6	6.121939	6.0019E-02	16.923264	03:42:53
7	7.171576	7.0310E-02	17.758286	04:01:33
8	8.181797	8.0214E-02	18.291721	04:12:01
9	9.207543	9.0270E-02	18.811863	04:22:46
10	10.24364	1.0043E-01	19.300762	04:33:15
11	12.80709	1.2556E-01	20.364176	04:55:43
12	15.30221	1.5002E-01	21.019983	05:07:57
13	17.85461	1.7505E-01	21.652704	05:20:14
14	20.41324	2.0013E-01	22.206797	05:31:33
15	22.98111	2.2530E-01	22.759758	05:44:08
16	25.57092	2.5070E-01	23.266424	05:56:28
17	28.23806	2.7684E-01	23.733496	06:08:45
18	30.69800	3.0096E-01	24.193924	06:22:41
19	33.16856	3.2518E-01	24.561995	06:34:02
20	35.83017	3.5128E-01	24.961493	06:47:34
21	38.27862	3.7528E-01	25.286472	06:58:58
22	40.98801	4.0184E-01	25.645184	07:13:13
23	43.50966	4.2657E-01	25.928568	07:23:55
24	46.09563	4.5192E-01	26.192924	07:33:58
25	48.46007	4.7510E-01	26.352404	07:39:08
26	51.18119	5.0178E-01	26.626532	07:50:57
27	53.56105	5.2511E-01	26.767750	07:56:00
28	56.10210	5.5002E-01	26.924028	08:01:05
29	58.66073	5.7511E-01	27.086632	08:07:42
30	61.22182	6.0021E-01	27.251503	08:13:39
31	63.85551	6.2603E-01	27.465488	08:23:48
32	66.31315	6.5013E-01	27.589767	08:28:35
33	68.88763	6.7537E-01	27.740885	08:35:05
34	71.41868	7.0018E-01	27.876698	08:40:51
35	73.99516	7.2544E-01	28.006769	08:46:38
36	76.55207	7.5051E-01	28.114141	08:50:49
37	79.09900	7.7548E-01	28.246387	08:56:36
38	81.63239	8.0032E-01	28.315231	08:59:21
39	84.18754	8.2537E-01	28.430307	09:02:45
40	86.70561	8.5005E-01	28.557039	09:08:41
41	89.26054	8.7510E-01	28.647200	09:13:50
42	91.81430	9.0014E-01	28.781427	09:20:05
43	94.38532	9.2535E-01	28.878681	09:24:38
44	96.91404	9.5014E-01	28.990353	09:30:51
45	99.49335	9.7542E-01	29.071613	09:35:36
46	101.52681	9.9536E-01	29.120001	09:37:50

Table S2. Raw data for C_3H_8 adsorption isotherms of BSF-4 at 298 K

	Adsorption			
SN	Pressure [KPa]	Relative pressure [P/Po]	Volume [cc/g]	Time [H:M:S]
1	1.027177	1.0070E-02	12.890207	00:47:03
2	2.074563	2.0339E-02	17.806271	00:53:43
3	3.080828	3.0204E-02	20.207922	00:58:30
4	4.147473	4.0661E-02	21.833076	01:03:53
5	5.115164	5.0149E-02	22.882885	01:08:11
6	6.163242	6.0424E-02	23.743679	01:11:57
7	7.201774	7.0606E-02	24.434776	01:16:04
8	8.164333	8.0042E-02	24.966707	01:19:30
9	9.280987	9.0990E-02	25.494463	01:23:41
10	10.20227	1.0002E-01	25.869400	01:26:35
11	12.86588	1.2614E-01	26.738649	01:30:49
12	15.43364	1.5131E-01	27.406672	01:35:43
13	17.86611	1.7516E-01	27.926247	01:39:10
14	20.41176	2.0012E-01	28.393705	01:42:32
15	22.95203	2.2502E-01	28.802870	01:45:55
16	25.67485	2.5171E-01	29.188080	01:50:44
17	28.06343	2.7513E-01	29.483459	01:54:02
18	30.63540	3.0035E-01	29.781368	01:56:57
19	33.17203	3.2522E-01	30.059204	02:00:33
20	35.71737	3.5017E-01	30.302940	02:03:52
21	38.28279	3.7532E-01	30.543905	02:06:49
22	40.81820	4.0018E-01	30.757469	02:09:38
23	43.37405	4.2524E-01	30.958042	02:12:35
24	45.92309	4.5023E-01	31.159897	02:15:46
25	48.50620	4.7555E-01	31.354250	02:19:04
26	51.08248	5.0081E-01	31.533096	02:21:49
27	53.62373	5.2572E-01	31.704287	02:24:52
28	56.18832	5.5087E-01	31.878098	02:27:46
29	58.73004	5.7578E-01	32.025177	02:30:38
30	61.24167	6.0041E-01	32.174461	02:33:46
31	63.81665	6.2565E-01	32.330616	02:37:08
32	66.34405	6.5043E-01	32.476147	02:40:14
33	68.94172	6.7590E-01	32.624763	02:43:16
34	71.44660	7.0046E-01	32.746124	02:45:56
35	74.00233	7.2551E-01	32.875320	02:49:02
36	76.58286	7.5081E-01	33.009659	02:52:22
37	79.07561	7.7525E-01	33.128914	02:55:43
38	81.64018	8.0039E-01	33.246986	02:58:43
39	84.21529	8.2564E-01	33.365417	03:01:30
40	86.73969	8.5039E-01	33.490253	03:04:34
41	89.29432	8.7543E-01	33.618599	03:08:06
42	91.84605	9.0045E-01	33.721203	03:10:43
43	94.42901	9.2577E-01	33.831409	03:13:20
44	96.93479	9.5034E-01	33.935600	03:15:59
45	99.48729	9.7537E-01	34.036846	03:18:55
46	101.30371	9.9317E-01	34.109283	03:21:22

Table S3. Raw data for C_3H_8 adsorption isotherms of BSF-9 at 308 K

	Adsorption			
SN	Pressure [KPa]	Relative pressure [P/Po]	Volume [cc/g]	Time [H:M:S]
1	1.022945	1.0029E-02	5.795971	01:17:25
2	2.042569	2.0025E-02	8.968955	01:48:00
3	3.071666	3.0114E-02	10.975419	02:14:24
4	4.103661	4.0232E-02	12.334906	02:35:58
5	5.130657	5.0301E-02	13.405576	02:56:28
6	6.136676	6.0163E-02	14.171387	03:11:08
7	7.174953	7.0343E-02	14.859057	03:26:22
8	8.223588	8.0623E-02	15.533664	03:45:43
9	9.229508	9.0485E-02	15.964916	03:56:10
10	10.22581	1.0025E-01	16.406971	04:08:08
11	12.85292	1.2601E-01	17.307459	04:29:26
12	15.32289	1.5022E-01	17.896084	04:41:31
13	17.92822	1.7577E-01	18.476299	04:56:03
14	20.49833	2.0096E-01	18.893684	05:04:54
15	23.05950	2.2607E-01	19.279234	05:13:43
16	25.58668	2.5085E-01	19.695765	05:26:12
17	28.17796	2.7625E-01	20.021177	05:35:46
18	30.87038	3.0265E-01	20.337206	05:45:29
19	33.28864	3.2636E-01	20.587540	05:53:02
20	35.71223	3.5012E-01	20.767031	05:58:02
21	38.25764	3.7507E-01	20.974991	06:03:40
22	40.80628	4.0006E-01	21.190519	06:10:45
23	43.38253	4.2532E-01	21.386143	06:17:07
24	45.90139	4.5001E-01	21.533997	06:21:43
25	48.45456	4.7504E-01	21.737455	06:28:55
26	51.04712	5.0046E-01	21.869724	06:33:06
27	53.59285	5.2542E-01	22.022915	06:38:18
28	56.30285	5.5199E-01	22.209473	06:45:22
29	58.71012	5.7559E-01	22.308035	06:48:40
30	61.21299	6.0013E-01	22.447311	06:55:15
31	63.76797	6.2518E-01	22.580099	07:00:35
32	66.35780	6.5057E-01	22.672575	07:04:44
33	68.85659	6.7506E-01	22.799282	07:10:19
34	71.42126	7.0021E-01	22.881786	07:13:06
35	74.00449	7.2553E-01	22.938915	07:15:43
36	76.54930	7.5048E-01	23.057245	07:19:11
37	79.06438	7.7514E-01	23.164896	07:24:14
38	81.64191	8.0041E-01	23.247253	07:27:47
39	84.17257	8.2522E-01	23.326254	07:31:04
40	86.72895	8.5028E-01	23.431585	07:35:59
41	89.28153	8.7531E-01	23.509378	07:39:32
42	91.84679	9.0046E-01	23.565594	07:42:36
43	94.39944	9.2548E-01	23.634075	07:46:12
44	96.93239	9.5032E-01	23.736498	07:50:31
45	99.48891	9.7538E-01	23.797400	07:53:22
46	101.44820	9.9459E-01	23.835655	07:55:39

Table S4. Raw data for C_3H_8 adsorption isotherms of BSF-4 at 308 K

		Adsorption		
SN	Pressure [KPa]	Relative pressure [P/Po]	Volume [cc/g]	Time [H:M:S]
1	1.134374	1.1121E-02	9.830808	00:45:38
2	2.058346	2.0180E-02	14.056192	00:51:03
3	3.062207	3.0022E-02	16.834999	00:56:20
4	4.124383	4.0435E-02	18.785007	01:01:39
5	5.103875	5.0038E-02	20.061264	01:05:46
6	6.157642	6.0369E-02	21.126472	01:10:04
7	7.188883	7.0479E-02	21.960913	01:13:57
8	8.224010	8.0628E-02	22.644875	01:18:18
9	9.191629	9.0114E-02	23.188875	01:22:10
10	10.30975	1.0108E-01	23.728462	01:26:31
11	12.86046	1.2608E-01	24.709129	01:30:45
12	15.30452	1.5004E-01	25.429806	01:34:18
13	18.00613	1.7653E-01	26.093090	01:38:23
14	20.41553	2.0015E-01	26.586979	01:42:15
15	23.12341	2.2670E-01	27.060936	01:46:15
16	25.52464	2.5024E-01	27.436249	01:49:40
17	28.05162	2.7502E-01	27.766253	01:52:58
18	30.61112	3.0011E-01	28.092867	01:56:36
19	33.17364	3.2523E-01	28.386324	02:00:12
20	35.71674	3.5016E-01	28.639999	02:03:16
21	38.29625	3.7545E-01	28.900827	02:06:45
22	40.82051	4.0020E-01	29.116350	02:10:05
23	43.40923	4.2558E-01	29.333372	02:13:12
24	45.95859	4.5057E-01	29.528835	02:16:21
25	48.48613	4.7535E-01	29.719065	02:19:00
26	51.05352	5.0052E-01	29.895695	02:21:52
27	53.58672	5.2536E-01	30.068617	02:24:51
28	56.17965	5.5078E-01	30.227530	02:27:44
29	58.69139	5.7541E-01	30.378857	02:30:22
30	61.22469	6.0024E-01	30.518902	02:32:56
31	63.81392	6.2563E-01	30.679108	02:36:09
32	66.35284	6.5052E-01	30.811733	02:38:53
33	68.93079	6.7579E-01	30.944687	02:42:17
34	71.47911	7.0078E-01	31.062250	02:45:21
35	73.98835	7.2538E-01	31.180994	02:48:20
36	76.59904	7.5097E-01	31.295891	02:50:57
37	79.13317	7.7582E-01	31.423092	02:54:00
38	81.66048	8.0059E-01	31.526194	02:57:21
39	84.23505	8.2583E-01	31.641747	02:59:57
40	86.79107	8.5089E-01	31.740860	03:03:01
41	89.28692	8.7536E-01	31.855713	03:05:38
42	91.84943	9.0048E-01	31.951902	03:08:41
43	94.41734	9.2566E-01	32.060318	03:11:24
44	96.95011	9.5049E-01	32.147774	03:15:04
45	99.51831	9.7567E-01	32.237236	03:17:57
46	101.36386	9.9376E-01	32.290234	03:19:52

Table S4. Raw data for C_3H_8 adsorption isotherms of BSF-9 at 288 K

	Adsorption			
SN	Pressure [KPa]	Relative pressure [P/Po]	Volume [cc/g]	Time [H:M:S]
1	1.028863	1.0087E-02	10.407788	01:55:28
2	2.041875	2.0018E-02	13.490642	02:34:21
3	3.075218	3.0149E-02	15.509540	03:10:16
4	4.104091	4.0236E-02	16.897552	03:39:47
5	5.128227	5.0277E-02	17.965418	04:05:04
6	6.143055	6.0226E-02	18.711298	04:22:32
7	7.167199	7.0267E-02	19.438675	04:40:51
8	8.162847	8.0028E-02	19.915344	04:51:16
9	9.216758	9.0360E-02	20.580242	05:10:25
10	10.23058	1.0030E-01	20.996386	05:20:51
11	12.81678	1.2565E-01	21.933697	05:42:31
12	15.32445	1.5024E-01	22.535461	05:54:34
13	17.87464	1.7524E-01	23.126057	06:06:36
14	20.44538	2.0044E-01	23.683538	06:19:33
15	23.00620	2.2555E-01	24.205572	06:31:59
16	25.55467	2.5054E-01	24.686687	06:44:13
17	28.32497	2.7770E-01	25.188902	06:57:31
18	30.67094	3.0070E-01	25.641537	07:11:26
19	33.23095	3.2579E-01	26.062271	07:24:14
20	35.78737	3.5086E-01	26.445705	07:37:20
21	38.36821	3.7616E-01	26.748461	07:45:50
22	40.90810	4.0106E-01	27.136103	08:00:23
23	43.65450	4.2799E-01	27.459803	08:12:03
24	45.90036	4.5000E-01	27.710991	08:20:53
25	48.44931	4.7499E-01	27.899855	08:26:07
26	51.15142	5.0148E-01	28.202423	08:37:34
27	53.56999	5.2520E-01	28.370287	08:43:16
28	56.12072	5.5020E-01	28.620075	08:53:41
29	58.68641	5.7536E-01	28.799301	09:00:03
30	61.23204	6.0031E-01	28.981527	09:06:38
31	63.93046	6.2677E-01	29.145857	09:12:28
32	66.64861	6.5342E-01	29.310017	09:17:57
33	68.88085	6.7530E-01	29.456701	09:22:58
34	71.40888	7.0009E-01	29.597952	09:28:04
35	73.98429	7.2534E-01	29.759132	09:33:41
36	76.50933	7.5009E-01	29.925844	09:39:48
37	79.06224	7.7512E-01	30.073706	09:45:48
38	81.62974	8.0029E-01	30.211010	09:51:14
39	84.16220	8.2512E-01	30.330215	09:55:49
40	86.74937	8.5048E-01	30.438902	09:59:00
41	89.29921	8.7548E-01	30.555571	10:03:49
42	91.81628	9.0016E-01	30.714546	10:10:05
43	94.43387	9.2582E-01	30.786200	10:12:51
44	96.95799	9.5057E-01	30.899466	10:16:48
45	99.47628	9.7526E-01	31.011896	10:20:52
46	101.44715	9.9458E-01	31.037745	10:22:47

Table S4. Raw data for C_3H_8 adsorption isotherms of BSF-4 at 288 K

	Adsorption			
SN	Pressure [KPa]	Relative pressure [P/Po]	Volume [cc/g]	Time [H:M:S]
1	1.022754	1.0027E-02	17.366718	00:48:12
2	2.054744	2.0145E-02	21.579187	00:53:55
3	3.106121	3.0452E-02	23.620960	01:00:14
4	4.093213	4.0130E-02	24.811432	01:04:49
5	5.142889	5.0420E-02	25.728174	01:09:24
6	6.562640	6.4340E-02	26.643110	01:13:43
7	7.433140	7.2874E-02	27.085848	01:16:46
8	8.323358	8.1602E-02	27.486872	01:20:12
9	9.254021	9.0726E-02	27.842405	01:23:10
10	10.29488	1.0093E-01	28.195587	01:25:56
11	12.87534	1.2623E-01	28.929333	01:30:39
12	15.44932	1.5146E-01	29.509045	01:34:23
13	17.87254	1.7522E-01	29.972027	01:37:33
14	20.42034	2.0020E-01	30.396738	01:41:03
15	22.99526	2.2544E-01	30.778866	01:44:07
16	25.64870	2.5146E-01	31.137796	01:49:15
17	28.06040	2.7510E-01	31.415249	01:52:08
18	30.63235	3.0032E-01	31.704245	01:55:31
19	33.20332	3.2552E-01	31.988201	01:58:50
20	35.72539	3.5025E-01	32.199532	02:01:36
21	38.27029	3.7520E-01	32.464291	02:06:09
22	40.86050	4.0059E-01	32.661366	02:08:48
23	43.35618	4.2506E-01	32.873203	02:12:29
24	45.94983	4.5049E-01	33.080265	02:15:29
25	48.51238	4.7561E-01	33.274147	02:20:04
26	51.05609	5.0055E-01	33.453445	02:22:56
27	53.61132	5.2560E-01	33.614376	02:25:33
28	56.17036	5.5069E-01	33.803043	02:28:25
29	58.73678	5.7585E-01	33.949539	02:30:56
30	61.28401	6.0082E-01	34.111931	02:35:24
31	63.81105	6.2560E-01	34.265045	02:38:13
32	66.36755	6.5066E-01	34.427231	02:41:32
33	68.87944	6.7529E-01	34.569050	02:44:07
34	71.44315	7.0042E-01	34.711422	02:46:46
35	74.01971	7.2568E-01	34.851662	02:50:47
36	76.56137	7.5060E-01	34.985199	02:53:43
37	79.10442	7.7553E-01	35.117435	02:56:34
38	81.67139	8.0070E-01	35.245079	02:59:33
39	84.19804	8.2547E-01	35.376137	03:02:39
40	86.75527	8.5054E-01	35.484043	03:05:18
41	89.32623	8.7575E-01	35.617012	03:09:04
42	91.83331	9.0033E-01	35.741970	03:12:08
43	94.38078	9.2530E-01	35.846985	03:15:06
44	96.93677	9.5036E-01	35.957047	03:17:55
45	99.50735	9.7556E-01	36.088814	03:20:41
46	101.31664	9.9330E-01	36.160328	03:22:59

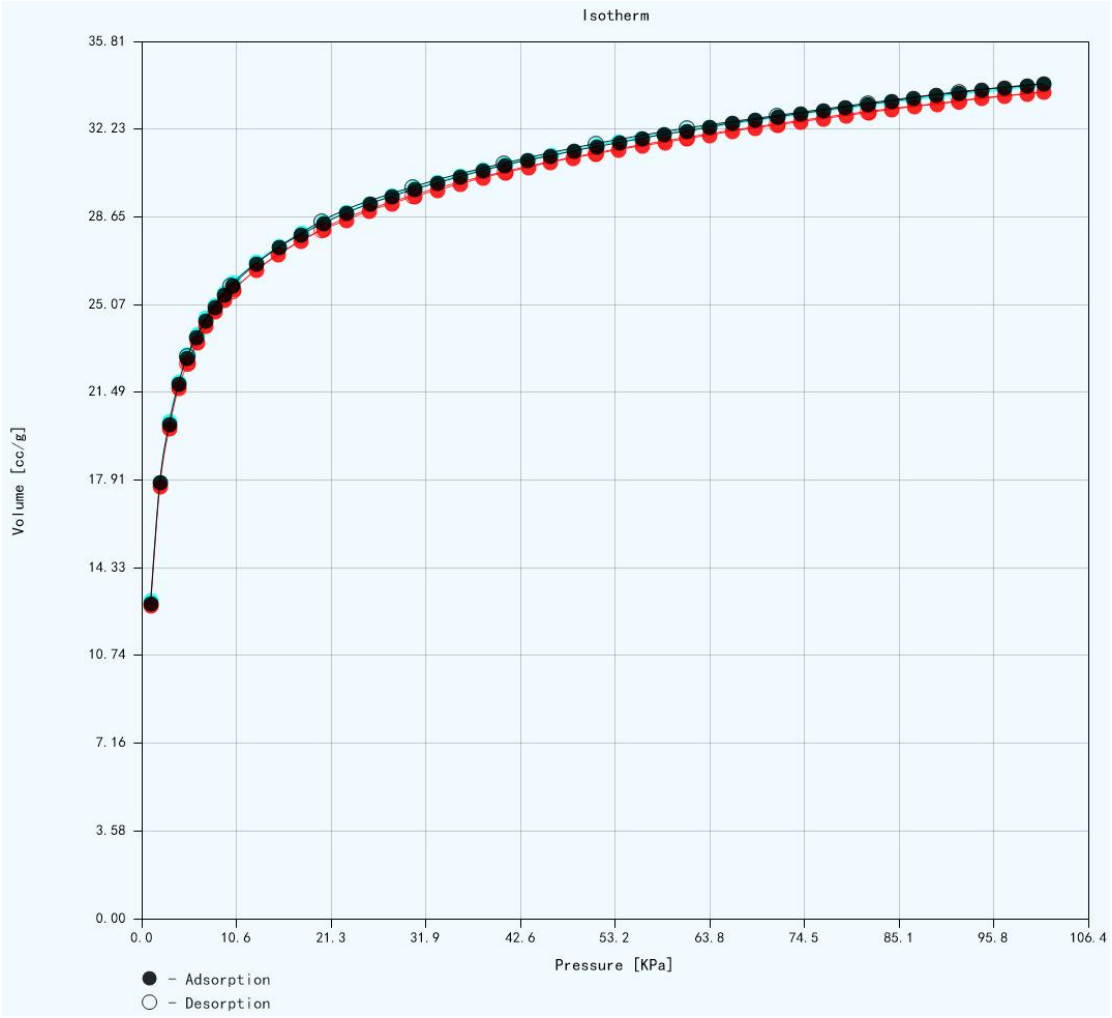

Figure S1. Repetitive measurement of C_3H_8 adsorption in BSF-4 at 298 K. Blue color curves represent the first adsorption-desorption cycle. Red color curves represent the second adsorption-desorption cycle where the sample was direct measured without any activation. Black color curves represent the third adsorption-desorption cycle where the sample was activated at 75 ºC for 30 min before measurement. The black circles nearly completely covered the blue color circles, indicating the good repeatability.

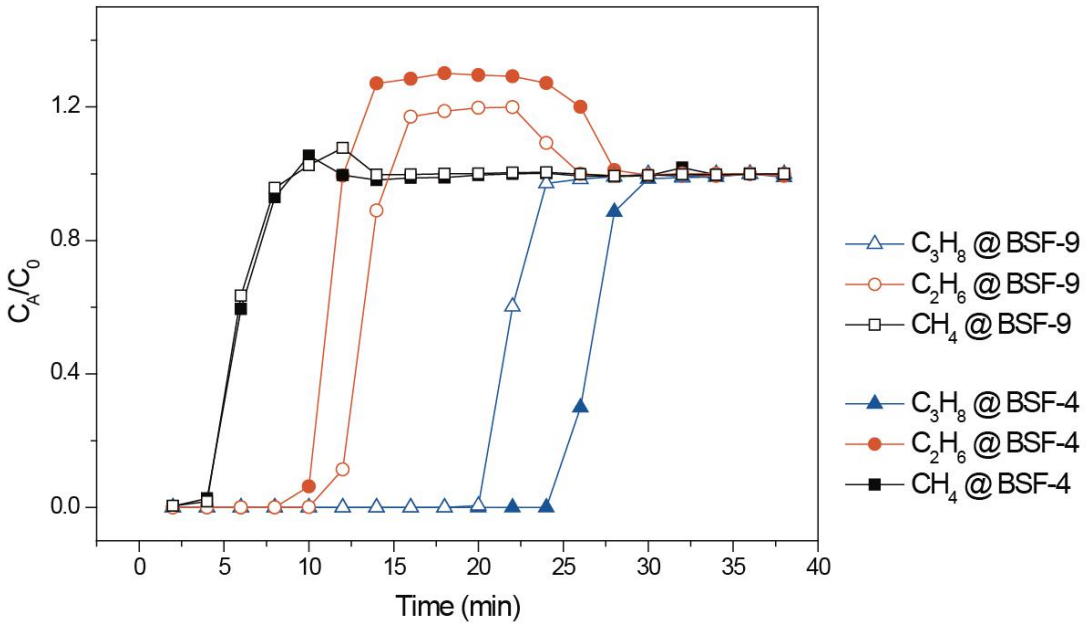

Figure S2. Experimental breakthrough curves of $C_3H_8/C_2H_6/CH_4$ (5/10/85) for BSF-9 and BSF-4. Fixed bed size: Φ 0.46 cm inner diameter × 5 cm length. Flow rate: 4 mL/min. BSF-9 loading: 0.32g. BSF-4 loading: 0.31g.